CST Particle Studio Simulations of Coaxial Multipactor and Comparison With Experiments

Stephen V. Langellotti, *Student Member, IEEE*, Nicholas M. Jordan, *Member, IEEE*, Y. Y. Lau, *Fellow, IEEE*, and Ronald M. Gilgenbach, *Life Fellow, IEEE*

***Abstract*— Using CST Particle Studio, we simulate the evolution of the multipactor, beginning with a single seed electron inside a coaxial waveguide. Upon impact with either the outer or inner metallic wall, the primary electron is removed and the emitted secondary electrons are allowed to have a realistic 3-D velocity distribution. It is found that the single electron evolves very quickly into an axisymmetric distribution. The radial distribution of the multipactoring electrons is broad and very different from the infinitesimally thin multipactor electron sheet that was often assumed in previous models. The simulated threshold voltage for the onset of multipactor was compared with published experiments, and the level of agreement was found to depend on the secondary electron yield model chosen.**

***Index Terms*— Coaxial transmission line, CST Particle Studio, multipactor, particle-in-cell (PIC).**

I. Introduction

MULTIPACTOR is a discharge phenomenon that occurs in radio frequency (RF) and microwave systems [1], [2]. It has been observed in microwave tubes [3], RF windows [4]–[7], coupling structures [8], antennae and transmission lines [9], [10], and in accelerator structures [11]–[13]. While the phenomenon is occasionally beneficial, it is much more frequently disruptive and even damaging [1]. Multipactor can cause loading of microwave cavities [14], localized heating of RF windows, and reduction in the signal quality [15]. These effects lead to performance degradation and possible destruction of the device [1], [2].

Multipactor can occur whenever RF power is transmitted along conductive surfaces in a vacuum [1], [2]. For example, consider the simple case of a parallel plate waveguide with an RF electric field normal to the surface. A free-electron near one of these plates (liberated, for example, by a cosmic ray) will be accelerated to the opposite plate by a favorable phase of the RF electric field [1], [2]. Upon impact, some number of secondary electrons will be released and, as the RF field reverses, accelerated back to the first surface. If the electron transit time is roughly in-phase with half an RF-cycle, this process will repeat itself every RF period, leading to exponential growth in the electron population [1], [2]. Eventually, space charge and loading effects will slow the electron population growth and the discharge will reach saturation [2]. This article is concerned primarily with the initial onset of multipactor before the electron population is sufficient to introduce saturation effects. Multipactor can also occur along a single surface and on dielectrics [2], but these cases are beyond the scope of this article.

Secondary electron emission drives multipactor [1]. The magnitude of the secondary emission yield (SEY) will determine if a discharge can occur. Low SEY materials are less likely to multipact and are often used for multipactor suppression [1], [2]. To maintain a multipactor discharge, the SEY for electrons impacting the surfaces must be greater than unity. Typically, the SEY is a strong function of the impact energy and has two major thresholds: the first and second crossover energies which represent the minimum and maximum incident energies where the SEY is unity. Particles whose energy is between the two crossover points have an SEY greater than unity and are responsible for multipactor growth [1], [2]. Another constraint for multipactor discharges is that the electrons must be in a stable phase relative to the RF field [1], [2]. This resonance condition was described analytically by Vaughan for the simple parallel plate case [1]. He also found that the multipactor breakdown voltage is proportional to $(fd)^2$ where f is the frequency and d is the separation between the electrodes [1]. This scaling rule is consistent with experiments performed by Woo 20 years earlier [16].

At the University of Michigan, we have built an experiment to investigate the onset of multipactor in a coaxial geometry and at higher frequencies than previously reported experimentally. The susceptibility diagram for the onset of multipactor is a plot of the threshold RF voltage versus fd, where f is the frequency and d is the gap spacing. Ideally, such a diagram would be used to design our experiment and predict when multipactor will occur. For coaxial structures, very few experimental susceptibility diagrams are available in the open literature other than those of Woo [16] and Graves [17], and their data are restricted to $fd < 4$ GHz $\cdot$ mm. The theory of multipactor in the coaxial geometry is very difficult, because of the huge parameter space. There is no fully analytic solution for the electron trajectory. Furthermore, the electron

Manuscript received November 20, 2019; revised February 18, 2020; accepted March 1, 2020. Date of publication March 31, 2020; date of current version June 10, 2020. This work was supported in part by Air Force Office of Science Research Multi-University Research Initiative (AFOSR MURI) through Michigan State University under Grant FA9550-18-1-0062 and in part by L3Harris Electron Devices Division. The review of this article was arranged by Senior Editor D. A. Shiffler. *(Corresponding author: Y. Y. Lau.)*

The authors are with the Department of Nuclear Engineering and Radiological Sciences, University of Michigan, Ann Arbor, MI 48109 USA (e-mail: svlangel@umich.edu; jordann@umich.edu; yylau@umich.edu; rongilg@umich.edu).

Color versions of one or more of the figures in this article are available online at http://ieeexplore.ieee.org.

Digital Object Identifier 10.1109/TPS.2020.2981257

transit time from the inner to outer conductor is different from the transit time from the outer to the inner conductor of a coaxial transmission line. This leads to drastic idealization, such as the use of infinitely thin electron sheets, virtually in all semianalytic models to assess multipactor in a coaxial transmission line, as exemplified by the recent work [15]. Therefore, we must rely on simulations for our experimental design. However, we must mention that the new approach, using chaos theory by Siddiqi and Kishek [18], seems to offer the predictive capability for the onset of multipactor in a coaxial geometry. The nonstationary statistical approach by Lin *et al*. [9] may also be noted.

CST Particle Studio (CST PS) [19] is a particle-in-cell (PIC) code that includes secondary electron emission and has been used extensively for simulating RF vacuum electronics [20]–[22]. While other PIC codes have been successfully used to predict multipactor [23], we have evaluated the performance of CST PS for predicting multipactor in a coaxial transmission line with the goal of reconstructing Woo's experimental data [16]. We will use a variety of SEY models for these simulations [24], [25] and demonstrate the growth of multipactor from a single seed electron.

II. Simulation Parameters

CST offers several methods of simulating multipactor evolution: Spark 3-D which models RF breakdown, a particle tracking solver that ignores space charge, a PIC solver that includes space charge, and a PIC solver that excludes space charge [26]. For the purpose of this article, we analyze only the fourth operating mode. Multipactor saturation is believed to be largely driven by the growth of space charge during multipactor [2]. Therefore, calculating saturation effects in a multipactor discharge necessitates including space charge effects. In this article, we are only concerned with finding the multipactor threshold by determining the conditions that promote the initial electron population growth. During multipactor onset, the total space charge is very small and negligibly perturbs the electron trajectories. As a result, space charge can be safely ignored when simulating the beginning of the multipactor discharge.

Our simulations are divided into three major types: validation of CST's predictive capability for multipactor onset (Section V), multipactor evolution from a single seed electron (Section VI), and determination of susceptibility for existing experimental hardware (Section VII). For the first two cases, we will consider a simple, 1 cm long 50 Ω, coaxial transmission line, as shown in Fig. 1. A constant amplitude of 2.45-GHz excitation is applied to the waveguide port on one end of the transmission line and can exit through a waveguide port on the opposite end. When a variation in fd is required, the coaxial gap, d, is varied, but the ratio of the outer and inner conductor radii is held constant at $b/a = 2.3$. Electrons exiting through either port are lost, but minimal axial diffusion is observed on the relevant time scales (see Appendix A). Excluding the single seed electron case, the vacuum region is initially seeded with 10 000 electrons. These particles are randomly distributed in position, direction, and energy.

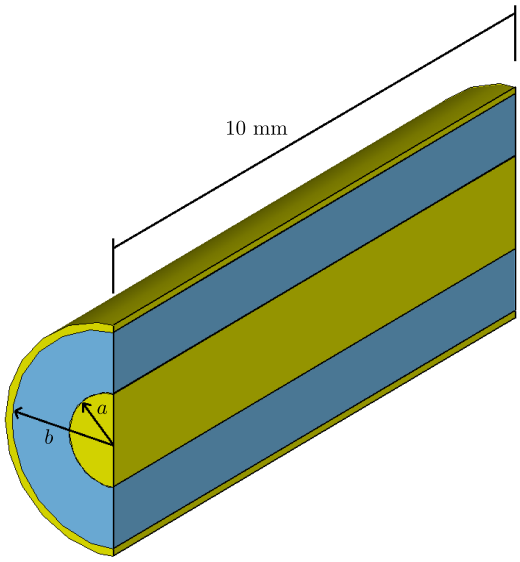

Fig. 1. CAD rendering of the simple coaxial model used in the simulations. The line impedance is held constant at 50 Ω with $b/a = 2.3$.

The initial electron energy ranges uniformly from 10^{-4} to 10 eV. All surfaces are copper, and the critical role of surface purity is examined in Section V.

CST provides two built-in methods to calculate SEY [26], the Vaughan [27] and Furman and Pivi [24] models; both are semiempirical formulations for the SEY as a function of the incident electron energy. In addition, rather than calculating SEY from a set of parameters, CST allows direct importation of tabulated SEY data. For the simulations discussed in Section V, the direct importation method is utilized. While the Vaughan model only considers the total electron emission [27], the Furman model also considers electron rediffusion, backscattering, and true secondary emission [24]. While the Furman model is more comprehensive, it also requires more knowledge of the material properties, and its 44 fitting parameters are available for few materials. In addition, the Furman model provides a probability distribution function (PDF) for the emission energy of secondary particles [24]. When using the Vaughan model or an imported SEY curve, CST assumes an emission energy distribution that is gamma distributed and weighted by a temperature [26]. For the simulations in this article, we have assumed a temperature of 7.5 eV, which provides an emission energy probability distribution function similar to the Furman model for copper. Secondary electrons are emitted at angles relative to the surface normal with the probability distribution function [26]

$$f(\theta) = \cos(\theta), \quad \theta \in [0, \pi/2]. \tag{1}$$

Simulations were conducted on a PC with a 10-core Intel i9 processor and using a Nvidia Tesla K40 GPU accelerator. Note that CST does not allow the usage of the GPU accelerator in simulations utilizing the Furman SEY model. Typical simulation times (to generate a full susceptibility diagram) were on the order of a few hours to a day.

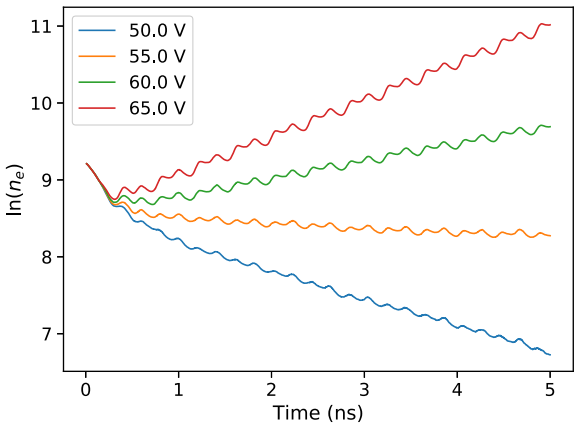

Fig. 2. Exponential growth and decay of the electron population at various gap voltage amplitudes. These simulations were produced with $fd = 1.0$ GHz · mm ($f = 2.45$ GHz, $d = 0.41$ mm) using SEY data for nonbaked copper [25].

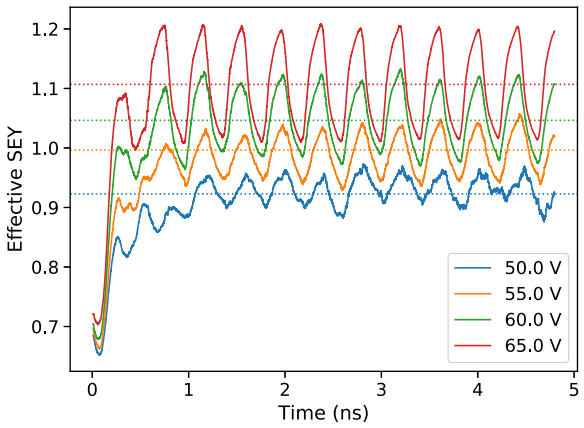

Fig. 3. Evolution of the effective secondary emission yield during multipactor. Dashed lines represent the average SEY over the last RF cycle. These simulations were produced with $fd = 1.0$ GHz · mm ($f = 2.45$ GHz, $d = 0.41$ mm).

III. Determination of Susceptibility

As noted previously, a multipactor discharge causes the electron population to increase exponentially. An example of this is shown in Fig. 2 at several applied voltage levels, with $fd = 1$ GHz · mm. For all applied voltages, an initial drop in electron population is observed as the randomly seeded electrons with unfavorable phase and velocity are absorbed by the boundaries. After this initial drop, in the 60- and 65-V cases, the electron population is clearly increasing, suggesting that the system is actively multipacting. Conversely, when the applied voltage is only 50 V, the electrons steadily decrease and there is no multipactor discharge. However, when the amplitude of the RF voltage is 55 V, the electron population is slowly shrinking, suggesting this voltage is close to the multipactor threshold.

To determine the voltage threshold necessary to initiate multipactor, we must quantitatively define evolution of the electron population. One way to represent this growth is with

$$n_e(t+\tau) = n_e(t)\delta(t), \quad n_e(0) = n_0 \tag{2}$$

where $n_e(t)$ is the electron population at time t, n_0 is the initial electron population, τ is the time scale of a multipactoring electron, from its birth on one surface to its impact on the opposite surface, and $\delta(t)$ is the effective secondary emission at time t. If we assume that the transmission line is undergoing first order, two-surface multipactor, then $\tau \approx T_{rf}/2$ where T_{rf} is the RF period [1]. Equation (2) states that the electron population at any time is a factor of δ higher than it was half an RF period earlier. Note that the temporal evolution of $\delta(t)$ may be obtained from the numerical data of $n_e(t)$

$$\delta(t) = \frac{n_e(t+\tau)}{n_e(t)}. \tag{3}$$

Fig. 3 shows the secondary emission yield that is obtained using this method. The SEY quickly develops into a steady oscillation that repeats every RF cycle. When we take the average of the last RF cycle, we obtain the values noted by the dashed lines in Fig. 3. For the 55-V case, we see that the average effective SEY is very nearly unity. This agrees with our observation that the system is almost, but not quite, multipacting (see Fig. 2). The time-average secondary emission yield is sufficient for predicting multipactor because it suggests a general trend of growth or decay over many RF cycles. This article is only concerned with finding the conditions that trigger stable, growing multipactor discharges. In addition, the oscillations in Fig. 3 are due to alternation between electron collisions with the inner and outer conductors. This periodic phenomenon is discussed in more detail in Section VI.

To construct a susceptibility diagram, we calculate the average effective SEY as a function of the applied voltage using the method outlined above. We then linearly interpolate this result to find the voltage where $\delta = 1$. This is the multipactor breakdown voltage. This procedure is repeated for a range of fd values to construct a susceptibility curve and is the simulation analog of the commonly used experimental method of steadily increasing RF power until multipactor is observed.

IV. Convergence Study

A convergence study was performed to determine the mesh density necessary to resolve our system. In CST, mesh density is controlled by specifying the minimum number of cells per unit wavelength. The effective SEY and susceptibility were calculated for a range of cells per wavelength (CPW) values. This article was performed with $fd = 1$ GHz · mm and used the nonbaked SEY data (discussed in Section V) imported directly into CST [25].

The results of the convergence study are shown in Fig. 4, where we show the effective secondary yield plotted as a function of the applied RF voltage. This figure shows that subsequent refinements beyond CPW = 30 change the SEY value by less than one percent, and each curve in Fig. 4 is nearly overlapping, suggesting that the simulations have reached a converged result. Based on this convergence study, we have chosen CPW = 30 for all simulations.

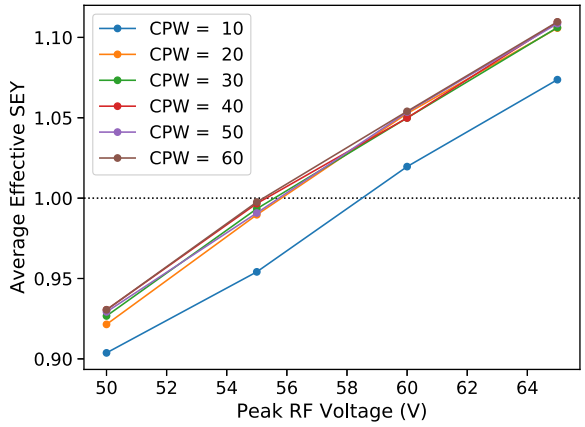

Fig. 4. Average effective SEY as a function of the applied peak RF voltage plotted for several values for the number of CPW.

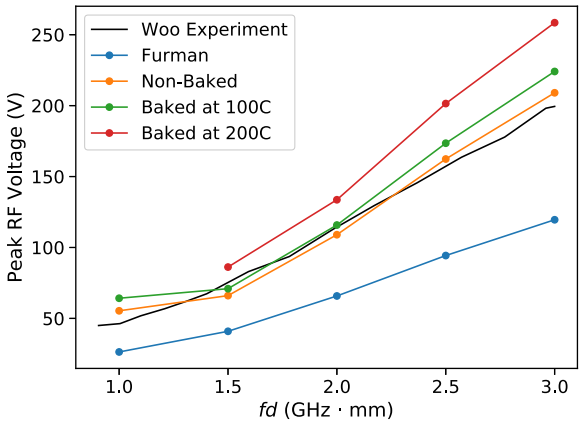

Fig. 6. Susceptibility for several surface treatments and comparison to Woo's experiment.

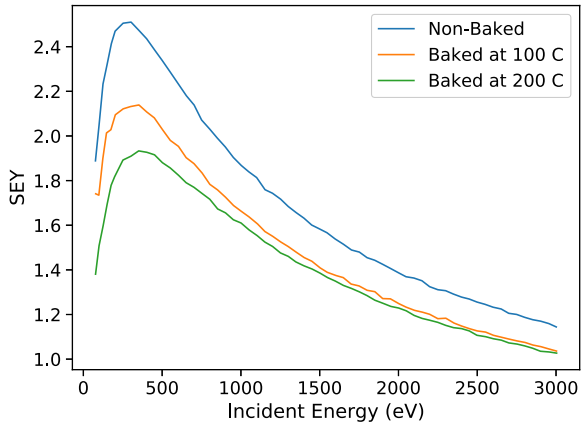

Fig. 5. Experimental SEY data from Bojko *et al.* [25] used in this article.

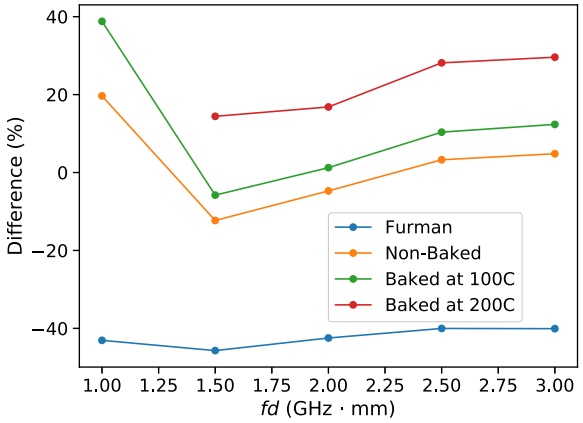

Fig. 7. Difference in simulated susceptibility data relative to Woo's experiment.

V. Susceptibility Simulation Results

Whether or not a device will undergo multipactor is highly dependent on the SEY properties of its constituent materials. Extensive studies have found that a material's SEY is highly dependent on its surface treatments, whether it is air exposure [25], thermal treatments [25], surface texture effects [28], or electron bombardment [29]. Copper SEY data in Fig. 5, from Bojko *et al.* [25], illustrate the strong dependence on surface conditions. In these experiments, the copper was "chemically cleaned" using a perchloroethylene solvent and an alkaline cleaning agent in an ultrasonic cleaner [30], then baked at various temperatures for 24 h [25].

Initial attempts at utilizing the Furman model, populated with Furman's coefficients for copper from [24], did not provide good correlation with Woo's experimental results [16]. As shown in Fig. 6, Furman's model consistently underpredicts the breakdown voltage by more than 40%. This poor agreement is likely due to differences between the surface conditions of the copper used to obtain Furman's model and the copper used in Woo's experiment. Note that this type of disagreement has been observed using other PIC codes and typically requires the SEY model to be adjusted [23]. When we supply CST with SEY data imported from [25], however, we find a surface condition (chemically cleaned, no bake out) which closely resembles Woo's copper data. As shown in Fig. 7, this agreement is particularly strong at higher values of fd, which is the region of interest for our experimental design. By abrasively cleaning the copper (as in [16]), or chemically cleaning the copper (as in [25]), the surface oxide layer and surface contaminants are removed and presumably comparable surface conditions are achieved.

VI. Multipactor Evolution

We next simulate the evolution of multipactor from a single seed electron. This simulation was performed with $fd = 2$ GHz · mm and the nonbaked SEY data from [25]. The initial velocity, phase, and position of the seed electron were determined through trial and error to ensure it will initiate the multipactor. The peak RF voltage was set to 120 V, slightly above the observed multipactor threshold of 115 V for copper [16]. Space charge effects were not considered in this simulation.

Fig. 8 shows the growth of the electron population as a multipactor discharge evolves. We begin with a single seed electron. After only a few RF periods, the electron cloud tends towards azimuthally uniform. This is consistent with the results from experiments described by Graves [17].

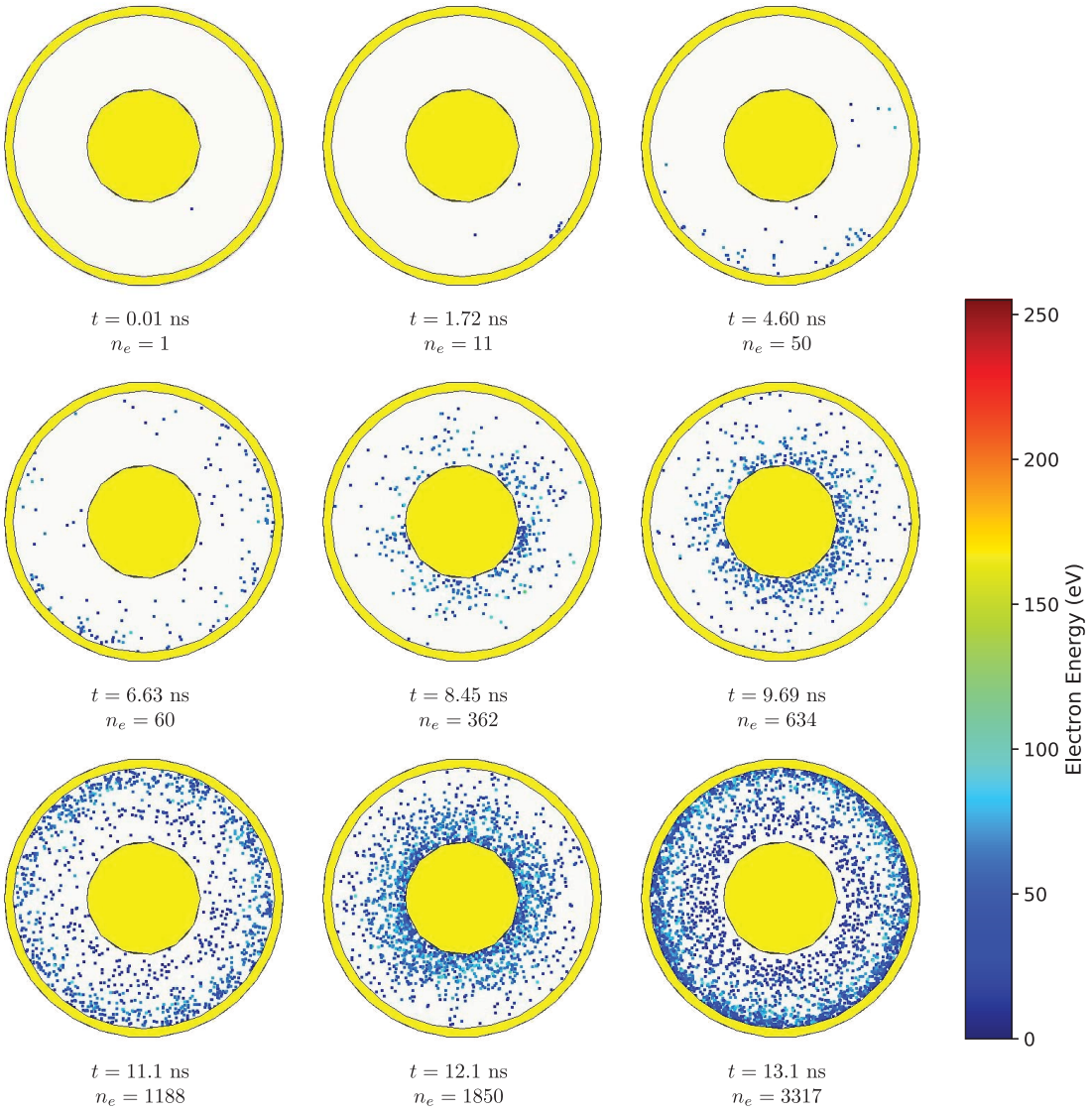

Fig. 8. Evolution of the multipactor discharge from a single seed electron with $fd = 2$ GHz $\cdot$ mm, $f = 2.45$ GHz, $a = 0.63$ mm, and $b = 1.44$ mm.

Fig. 9 shows the energy distribution of particles incident on the inner and outer conductors. These distributions are cumulative over the full simulation duration (20 ns) and are dominated by the later time steps where the electron population is very large. This plot suggests the multipactor growth is primarily driven by the outer conductor. On average, electrons impact the outer conductor at higher energies beyond the first crossover point in the SEY curve and, thus, have a higher SEY coefficient. On the other hand, the electrons impacting the inner conductor have an average energy below the first crossover point. As shown in Fig. 3, the SEY oscillates between a high value and a low value. The peaks occur when the electrons are incident on the outer conductor. Conversely, the low values coincide with impacts against the inner conductor. These combined effects lead to an average SEY that is slightly above unity. These general trends are consistent with previous studies which used the highly idealized model of infinitesimally thin sheets of multipacting electrons with monoenergetic emission velocities [15], [31], [32].

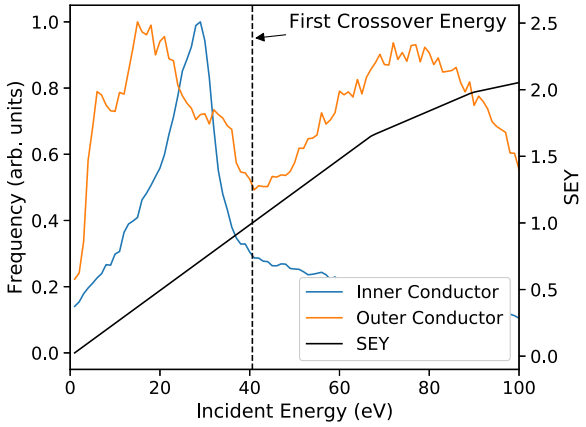

Fig. 9. Energy distribution and SEY for particles interacting with the coax surfaces.

An additional simulation was performed to demonstrate the effects of space charge on the multipactor discharge. The RF voltage was set to 120 V, and $fd =$ 2 GHz $\cdot$ mm

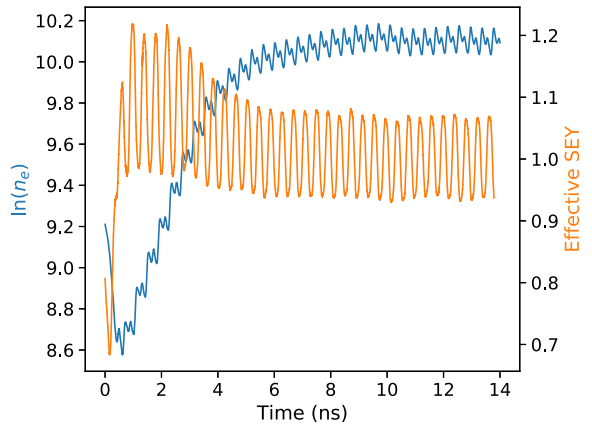

Fig. 10. Evolution of the electron population and effective SEY during a saturated multipactor discharge.

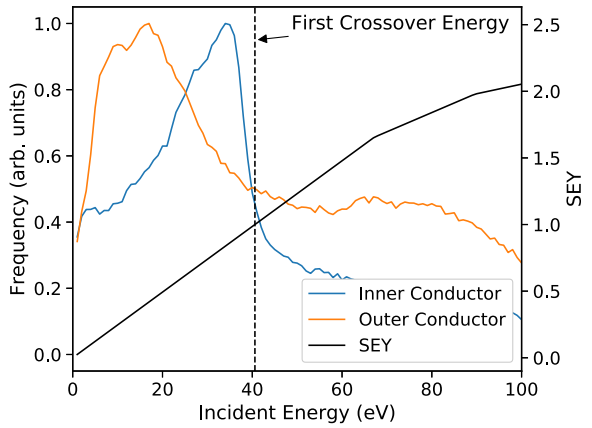

Fig. 11. Energy distribution and SEY for particles interacting with the coax surfaces for a saturated multipactor discharge.

($f = 2.45$ GHz, $d = 0.82$ mm). The multipactor discharge was seeded with 10 000 electrons with random energy, direction, and position. To improve computational efficiency, each simulation particle was weighted with the mass and charge of 10 000 electrons. Fig. 10 shows the resulting growth of the electron population and the effective SEY (calculated in the manner described in Section III). After the initial loss of unfavorable electrons, the electron population grows, just as in the no-space-charge case. However, after 4 ns, the growth begins to slow down as the space charge builds up. Note that the effective SEY also approaches unity as the discharge saturates.

When we examine the energy distribution for particles colliding with the electrodes (shown in Fig. 11), we see why the discharge stops growing. As the discharge reaches saturation, the energy of particles hitting the outer conductor is significantly decreased; most of these particles are now below the first crossover energy. Therefore, these electrons are now no longer driving the growth of the discharge. The rapid saturation of this discharge (~8 ns), compared to the simulation in Fig. 8 (unsaturated until after over 13 ns), is due to the 10 000× weighting factor, 10 000 seed electrons, and the inclusion of space-charge effects.

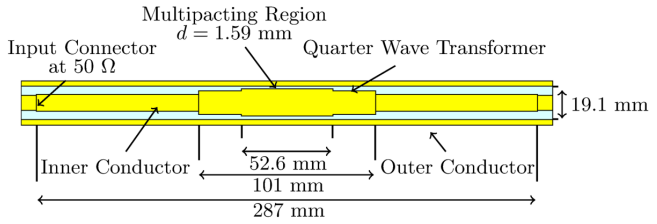

Fig. 12. Cross section of the coaxial transmission line in a planned experiment.

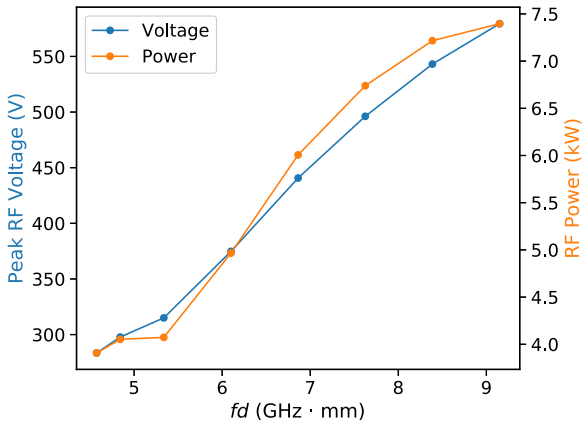

Fig. 13. Predicted breakdown voltage and power for the experimental configuration.

VII. Experimental Design

With our CST model capable of approximately reproducing experimental data, we expand this model to predict the multipactor threshold for other geometries of interest. A cross section of the coaxial experimental geometry is shown in Fig. 12. In the multipacting region (center), the gap is $d = 1.59$ mm. Other segments of the transmission line have a larger value for d and, thus, a larger voltage threshold for multipactor. On either side of the multipacting segment are quarter-wave transformers. These ensure an impedance match between the multipacting region and the 50- Ω straight coaxial segments on either side. The edges of the simulation volume are 50- Ω coaxial ports for injection of a 3.05-GHz RF excitation.

The simulated breakdown voltage and power for the experimental configuration are shown in Fig. 13. For the designed gap ($d = 1.59$ mm, $fd = 4.84$ GHz · mm), we predict multipactor to occur at 298 V and 4.1 kW when we use the nonbaked SEY data [25]. Thus, an experimental investigation of multipactor should be possible with a 5 kW, 3.05-GHz RF source.

VIII. Conclusion

This article has investigated the efficacy of using CST Particle Studio for predicting multipactor breakdown in coaxial transmission lines. Our simulations have demonstrated that the SEY model is critical for accurately predicting multipactor. When we use experimental SEY data for nonbaked copper, CST Particle Studio is able to reproduce some of Woo's

published experimental data. In addition, when we examine the evolution of the multipactor discharge, we see some behavior consistent with previous theoretical and experimental studies. This has allowed us to proceed with our experimental design using realistic simulation models.

APPENDIX A
AXIAL DIFFUSION OF MULTIPACTING ELECTRONS

In this Appendix, we apply an elementary random walk analysis to show that axial diffusion is minimal for multipactoring electrons over the time scale of simulation. This analysis uses the classical description of diffusion due to random walk. A multipactoring electron, from its birth on a surface, has an equal probability of moving in the $+z$ and $-z$ directions. During its transit time to the opposite surface, Δt, it moves axially a distance $\Delta z = v_z \Delta t$, where v_z is the z-component of its emission velocity at birth. When it strikes the opposite surface, the next generation of multipactoring electrons will undergo similar random motions in the z-direction. From statistical mechanics, such a random walk process leads to axial diffusion of multipactoring electrons with the diffusion coefficient given by

$$D = \frac{(\Delta z)^2}{\Delta t} = v_z^2 \Delta t = \frac{v_z^2}{2f} \tag{A.1}$$

where we have assumed a first order, two-surface multipactor so that the transit time $\Delta t = 1/(2f)$ is one half of the RF period. From this diffusion coefficient D, we estimate the time scale (T) for diffusion over an axial distance (L) to be

$$T = \frac{L^2}{D} = \frac{2fL^2}{v_z^2}. \tag{A.2}$$

Numerically, (A.2) becomes

$$T = 0.569\ \mu\text{s} \times \left(\frac{f}{1\ \text{GHz}}\right) \times \left(\frac{L}{1\ \text{cm}}\right)^2 \times \left(\frac{1\ \text{eV}}{E_z}\right) \tag{A.3}$$

where $E_z = mv_z^2/(2e)$ denotes the energy (in eV) associated with the z-motion of a multipactoring electron.

In our simulation, $f = 2.45$ GHz, $L = 1$ cm, and if we take $E_z = 1$ eV, (A.3) gives $T = 1.4\ \mu$s, which is much longer than the time scales shown in Figs. 2, 3, 8, and 10.

REFERENCES

[1] J. R. M. Vaughan, "Multipactor," *IEEE Trans. Electron Devices*, vol. 35, no. 7, pp. 1172–1180, Jul. 1988.

[2] R. A. Kishek, Y. Y. Lau, L. K. Ang, A. Valfells, and R. M. Gilgenbach, "Multipactor discharge on metals and dielectrics: Historical review and recent theories," *Phys. Plasmas*, vol. 5, no. 5, pp. 2120–2126, May 1998.

[3] J. R. M. Vaughan, "Observations of multipactor in magnetrons," *IEEE Trans. Electron Devices*, vol. ED-15, no. 11, pp. 883–889, Nov. 1968.

[4] D. H. Preist and R. C. Talcott, "On the heating of output windows of microwave tubes by electron bombardment," *IRE Trans. Electron Devices*, vol. 8, no. 4, pp. 243–251, Jul. 1961.

[5] J. R. M. Vaughan, "Some high-power window failures," *IRE Trans. Electron Devices*, vol. 8, no. 4, pp. 302–308, Jul. 1961.

[6] S. Yamaguchi, Y. Saito, S. Anami, and S. Michizono, "Trajectory simulation of multipactoring electrons in an S-band pillbox RF window," *IEEE Trans. Nucl. Sci.*, vol. 39, no. 2, pp. 278–282, Apr. 1992.

[7] Y. Saito, S. Michizono, S. Anami, and S. Kobayashi, "Surface flashover on alumina RF windows for high-power use," *IEEE Trans. Electr. Insul.*, vol. 28, no. 4, pp. 566–573, Aug. 1993.

[8] G. Gevanz, "Multipactor simulations in superconducting cavities and power coupler," *Phys. Rev. ST Accel. Beams*, vol. 4, no. 1, Jan. 2001, Art. no. 012001.

[9] S. Lin *et al.*, "Multipactor threshold calculation of coaxial transmission lines, in microwave applications with nonstationary statistical theory," *Phys. Plasmas*, vol. 22, no. 8, Aug. 2015, Art. no. 082114, doi: 10.1063/1.4928421.

[10] D. Gonzalez-Iglesias, O. Monerris, B. G. Martinez, M. E. Diaz, V. E. Boria, and P. M. Iglesias, "Multipactor RF breakdown in coaxial transmission lines with digitally modulated signals," *IEEE Trans. Electron Devices*, vol. 63, no. 10, pp. 4096–4103, Oct. 2016.

[11] S. Humphries, *Principles of Charged Particle Acceleration*. Mineola, NY, USA: Dover, 1986.

[12] L. Wu and L. K. Ang, "Multipactor discharge in a dielectric-loaded accelerating structure," *Phys. Plasmas*, vol. 14, no. 1, Jan. 2007, Art. no. 013105, doi: 10.1063/1.2435709.

[13] J. G. Power *et al.*, "Observation of multipactor in an alumina-based dielectric-loaded accelerating structure," *Phys. Rev. Lett.*, vol. 92, no. 16, Apr. 2004, Art. no. 164801.

[14] R. Kishek and Y. Y. Lau, "Interaction of multipactor discharge and RF circuit," *Phys. Rev. Lett.*, vol. 75, no. 6, pp. 1218–1221, Aug. 1995.

[15] P. Y. Wong, Y. Y. Lau, P. Zhang, N. Jordan, R. M. Gilgenbach, and J. Verboncoeur, "The effects of multipactor on the quality of a complex signal propagating in a transmission line," *Phys. Plasmas*, vol. 26, no. 11, Nov. 2019, Art. no. 112114, doi: 10.1063/1.5125408.

[16] R. Woo, "Multipacting discharges between coaxial electrodes," *J. Appl. Phys.*, vol. 39, no. 3, pp. 1528–1533, Feb. 1968.

[17] T. P. Graves, "Experimental investigation of electron multipactor discharges at very high frequencies," Ph.D. dissertation, Massachusetts Inst. Technol., Cambridge, MA, USA, 2006.

[18] M. Siddiqi and R. Kishek, "A predictive model for multipactor discharge in coaxial systems based on chaos theory," *IEEE Trans. Electron Devices*, vol. 66, no. 10, pp. 4403–4407, Oct. 2019.

[19] *CST Studio Suite*, Dassault Systems, Vélizy-Villacoublay, France 2019.

[20] U. Singh, N. Kumar, N. Kumar, A. Kumar, and A. K. Sinha, "Three-dimensional simulation of triode-type MIG for 1MW, 120GHz gyrotron for ECRH applications," *Infr. Phys. Technol.*, vol. 55, no. 1, pp. 108–111, Jan. 2012.

[21] J.-H. Han and S.-K. Ryu, "Optimal operating conditions based on mode competition for maximum efficiency of double-strapped magnetron," *IEEE Trans. Plasma Sci.*, vol. 47, no. 7, pp. 3160–3167, Jul. 2019.

[22] D. Safi, P. Birtel, S. Meyne, and A. F. Jacob, "A traveling-wave tube simulation approach with CST particle studio," *IEEE Trans. Electron Devices*, vol. 65, no. 6, pp. 2257–2263, Jun. 2018.

[23] V. E. Semenov, N. Zharova, R. Udiljak, D. Anderson, M. Lisak, and J. Puech, "Multipactor in a coaxial transmission line. II. Particle-in-cell simulations," *Phys. Plasmas*, vol. 14, no. 3, Mar. 2007, Art. no. 033509, doi: 10.1063/1.2710466.

[24] M. A. Furman and M. T. F. Pivi, "Probabilistic model for the simulation of secondary electron emission," *Phys. Rev. ST Accel. Beams*, vol. 5, no. 12, Dec. 2002, Art. no. 124404.

[25] I. Bojko, N. Hilleret, and C. Scheuerlein, "Influence of air exposures and thermal treatments on the secondary electron yield of copper," *J. Vac. Sci. Technol. A, Vac. Surf. Films*, vol. 18, no. 3, pp. 972–979, May 2000.

[26] *CST Studio Suite Help*, Dassault Systems, Vèlizy-Villacoublay, France, 2019.

[27] J. R. M. Vaughan, "A new formula for secondary emission yield," *IEEE Trans. Electron Devices*, vol. 36, no. 9, pp. 1963–1967, Sep. 1989.

[28] M. Ye *et al.*, "Suppression of secondary electron yield by micro-porous array structure," *J. App. Phys.*, vol. 113, no. 7, 2013, Art. no. 074904, doi: 10.1063/1.4792514.

[29] R. Cimino *et al.*, "Nature of the decrease of the secondary-electron yield by electron bombardment and its energy dependence," *Phys. Rev. Lett.*, vol. 109, no. 6, Aug. 2012, Art. no. 064801.

[30] C. Benvenuti *et al.*, "Surface cleaning efficiency measurements for UHV applications," *Vacuum*, vol. 53, nos. 1–2, pp. 317–320, May 1999.

[31] R. Udiljak, D. Anderson, M. Lisak, V. E. Semenov, and J. Puech, "Multipactor in a coaxial transmission line. I. analytical study," *Phys. Plasmas*, vol. 14, no. 3, Mar. 2007, Art. no. 033508, doi: 10.1063/1.2710464.

[32] E. Sorolla, A. Sounas, and M. Mattes, "Space charge effects for multipactor in coaxial lines," *Phys. Plasmas*, vol. 22, no. 3, Mar. 2015, Art. no. 033512, doi: 10.1063/1.4915130.

Stephen V. Langellotti (Student Member, IEEE) received the B.S. degree in nuclear engineering from North Carolina State University, Raleigh, NC, USA, in 2017, and the M.S.E. degree in nuclear engineering and radiological sciences from the University of Michigan, Ann Arbor, MI, USA, in 2019, where he is currently pursuing the Ph.D. degree with the Department of Nuclear Engineering and Radiological Sciences.

He is a former Reactor Operator for the PULSTAR nuclear reactor with North Carolina State University and was licensed by the United States Nuclear Regulatory Commission.

Nicholas M. Jordan (Member, IEEE) received the B.S.E., M.S.E., and Ph.D. degrees in nuclear engineering and radiological science from the University of Michigan, Ann Arbor, MI, USA, in 2002, 2004, and 2008, respectively.

From 2008 to 2013, he was with Cybernet Systems, Ann Arbor, where he developed technology to disable uncooperative vehicles using microwave pulses. He is currently an Assistant Research Scientist with the Plasma, Pulsed Power, and Microwave Laboratory, University of Michigan. His current research interests include high-power microwave devices, pulsed power, laser ablation, Z-pinch physics, and plasma discharges.

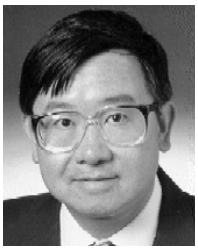

Y. Y. Lau (Fellow, IEEE) received the B.S., M.S., and Ph.D. degrees in electrical engineering from the Massachusetts Institute of Technology, Cambridge, MA, USA, in 1968, 1970, and 1973, respectively.

He is currently a Professor with the University of Michigan, Ann Arbor, MI, USA, where he is specialized in RF sources, heating, and discharge.

Dr. Lau was an elected Fellow of the American Physical Society in 1986. He received the 1999 IEEE Plasma Science and Applications Award and the 2017 IEEE John R. Pierce Award for Excellence in Vacuum Electronics. He served three terms as an Associate Editor for the *Physics of Plasmas* from 1994 to 2002.

Ronald M. Gilgenbach (Life Fellow, IEEE) received the B.S. and M.S. degrees from the University of Wisconsin, Madison, WI, USA, in 1972 and 1973, respectively, and the Ph.D. degree in electrical engineering from Columbia University, New York, NY, USA, in 1978.

He is currently the Chihiro Kikuchi Collegiate Professor with the Nuclear Engineering and Radiological Sciences Department, University of Michigan (UM), Ann Arbor, MI, USA. In the early 1970s, he spent several years as a Member of the Technical Staff at Bell Telephone Labs, Holmdel, NJ, USA. From 1978 to 1980, he performed gyrotron research with the Naval Research Lab (NRL), in DC and performed the first electron cyclotron heating experiments on a tokamak plasma in the USA with the Oak Ridge National Laboratory, Oak Ridge, TN, USA. He joined the faculty of the University of Michigan, in 1980, and founded the Plasma, Pulsed Power and Microwave Laboratory. At UM, he has supervised 51 graduated Ph.D. students and authored or coauthored some 200 journal articles.

Dr. Gilgenbach is a fellow of the American Physical Society Division of Plasma Physics and of the American Nuclear Society. He received the 1997 IEEE Plasma Sciences and Applications Committee (PSAC) Award and the 2017 IEEE Peter Haas Pulsed Power Award. He served as the IEEE PSAC Chair in 2007–2008. He is a past Associate Editor of the *Physics of Plasmas*.